Spontaneous Elastocapillary Winding of Thin Elastic Fibers in Contact with Bubbles

Adam Fortais,[1] Kathleen Charlesworth,[1] Rafael D. Schulman,[1] and Kari Dalnoki-Veress[1,2,*]
[1]Department of Physics and Astronomy, McMaster University, 1280 Main Street West, Hamilton, Ontario L8S 4M1, Canada
[2]UMR CNRS Gulliver 7083, ESPCI Paris, PSL Research University, 75005 Paris, France

(Received 2 August 2021; accepted 19 October 2021; published 18 November 2021)

We study the elastocapillary interaction between flexible microfibers in contact with bubbles trapped at the surface of a liquid bath. Microfibers placed on top of bubbles are found to migrate to and wrap into a coil around the perimeter of the bubble for certain bubble-fiber size combinations. The wrapping process is spontaneous: the coil spins atop the bubble, thereby drawing in excess fiber floating on the bath. A two-dimensional microfiber coil emerges which increases the lifetime of the bubbles. A simple model incorporating surface and bending energies captures the spontaneous winding process.

DOI: 10.1103/PhysRevLett.127.218001

Surface wetting is common to many natural and industrial processes like the clumping of wet hairs and fibers [1–5], and the spreading of liquids on surfaces [6–8], which can result in beautiful and useful elastic deformations of the solid surface [9–17]. Even simple systems consisting of a stiff fiber which is partially wet by a drop is more complicated than it may first appear, as it can take on two equilibrium states: an axisymmetric "barrel" where the fiber penetrates the drop, and a nonaxisymmetric "clamshell" configuration where the droplet is sessile on one side of the fiber [6,7,16,18–21]. More compliant fibers are able to buckle and collapse inside the drop when tension is reduced [5,22–26]. In some cases this process has been shown to result in spooling a fiber within a liquid drop, and is used by some types of spiders in web construction [25]. Alternatively, a droplet may take on a clamshell configuration when placed on a fiber if the liquid drop is small compared with the radius of the fiber, or if the fiber is less wettable [12,20,21,27]. In the clamshell configuration, capillary forces can be strong enough to induce large deformations in a thin strip or fiber [27], in some cases even causing the fiber to wrap entirely *around* the drop [12,28].

In all of these elastocapillary systems, where capillarity and elasticity compete, a natural length scale emerges which sets an approximate upper bound on the size of elastic deformations caused by capillary forces [16,17]. The bending elastocapillary length l_b represents the ratio between bending and capillary energies in a system, and for a fiber can be defined as $l_b = \sqrt{EI/2\pi r\gamma}$, where EI is the bending stiffness of the elastic fiber, $2\pi r$ is the circumference of the fiber, and γ is the liquid-vapor surface tension [16]. EI, which depends on Young's modulus of the fiber E and the second moment of area I, has a strong dependence on the radius of the elastic fiber r. For a uniform, cylindrical fiber, $I = \pi r^4/4$, which explains why elastocapillary deformations are easily observed in slender objects like thin fibers.

Here we explore the elastic deformation of a fiber due to capillary forces at a liquid bath with an air bubble. An elastic fiber is introduced at the liquid membrane at the top of an air bubble. If the fiber diameter is greater than the thickness of the film, the fiber bridges across the film, and, under some conditions, causes the fiber to spontaneously wind around the circular periphery of the liquid membrane. The resulting coil is shown in Figs. 1(a) and 1(b) before (a)

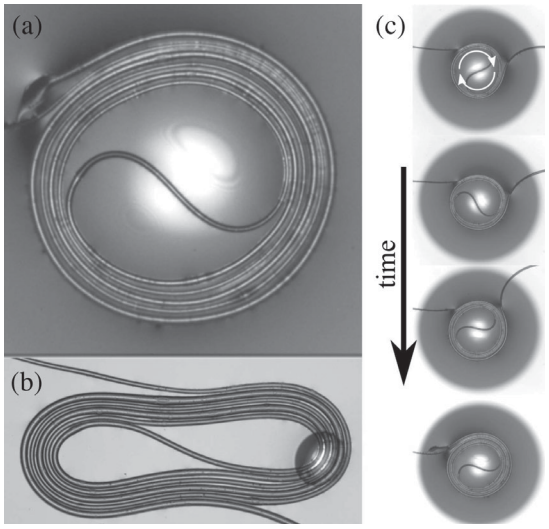

FIG. 1. An elastic fiber (SIS) with a radius $r = 5$ μm winds around the liquid film at the top of an air bubble at the interface of a glycerol bath before (a), and after (b), the bubble bursts [in this case a small air bubble remained trapped below the coils on the right side of (b)]. (c) A time sequence of the winding process. The fiber can coil spontaneously, forming structures like these in no more than 2–3 minutes. For scale, the diameter of the coil in (a) and (c) is ~500 μm.

and after the air bubble bursts (b) (video in Supplemental Material [29]). The bridging mechanism is reminiscent of Pickering emulsions and techniques for bubble stabilization involving the absorption of solid inclusions at the liquid interfaces [30–38]. In short, the fiber has a lower free energy when bridging the liquid film on the top of the bubble, compared with that at the liquid interface, where less fiber is in contact with air. Using a simple model which balances the energy cost of bending the fiber against the reduction in the surface energy when the fiber bridges the liquid film, we predict the onset of winding. This coiled structure bears a striking resemblance to the packing of genetic material within viral capsids, a process that requires large lengths of fiberlike materials to pack and orient within small volumes [39–42]. We observe that the wound structure stabilizes air bubbles at the interface.

In the experiment a fiber with radius $r \sim 10^{-6}$ m is placed on the surface of a glycerol ($\gamma \approx 64$ mN/m) bath. Small air bubbles with radii ranging from approximately $R_b \sim 10^{-4}$ to $R_b \sim 10^{-3}$ m are introduced below the surface of the bath with a syringe connected to a micropipette. Buoyancy carries the air bubbles to the surface, lifting the fiber as the bath's surface deforms locally into a shape well approximated by a spherical cap. A schematic of the air bubble is shown in Fig. 2(a). The air bubble and fiber are observed with optical microscopy from above [see Figs. 2(b)–2(g)]. Worth noting is that the bubble cap can be related to R_b through the Bond number, Bo, which relates the relative importance of gravity to surface tension. $\mathrm{Bo} = \rho g R_b^2/\gamma$, where $\rho \approx 1.3 \times 10^3$ kg/m^3 is the difference in density between the air and the liquid, and g is gravitational acceleration. Here $\mathrm{Bo} \ll 1$, and a bubble at the surface of a liquid will remain nearly spherical and protrude only about $\sim 0.05 R_b$ above the surface of the liquid [43–45].

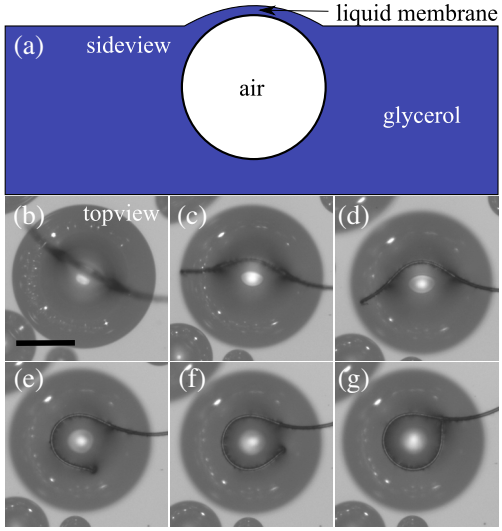

FIG. 2. (a) A schematic of an air bubble which deforms the surface of a liquid bath via buoyancy. (b)–(g) A SIS fiber spontaneously winding around an air bubble in a bath of glycerol over approximately 30 seconds. The scale bar is 200 μm.

The polymer fibers used in the experiment are made from several materials: polystyrene (PS), a glass at room temperature with a molecular weight of $M_n = 25000$ kg/mol and polydispersity index of 1.04 (Polymer Source Inc.); Elastollan 1185A-10 (BASF Inc.), a polyether-based physically cross-linked elastomeric solid at room temperature; and styrene-isoprene-styrene (SIS), a triblock copolymer (14% styrene content, Sigma-Aldrich) which is a physically cross-linked elastomeric solid at room temperature. The elastic modulus of Elastollan is $E_{\mathrm{elast}} = 10 \pm 3$ MPa (determined via extensional stress-strain tests performed on fibers with $r \sim 10^{-6}$ m). The elastic moduli of PS and SIS are taken from the literature ($E_{\mathrm{PS}} = 3.4$ GPa, $E_{\mathrm{SIS}} = 0.8$ MPa) [46,47]. Fibers are made by either melting or dissolving the polymer, dipping a glass pipette into the viscous polymer liquid, then rapidly pulling the pipette out of the polymer. PS and Elastollan were melted by heating a small sample (170 °C for PS and 235 °C for Elastollan), while the SIS was dissolved into toluene (Optima-grade, Sigma Aldrich) to form a viscous polymer solution. The resulting fibers have uniform, cylindrical cross sections with diameters ~ 10 μm, which were inspected optically for uniformity.

When a fiber and bubble come into contact, depending on the size of the air bubble and fiber, one of two processes occur. Either the fiber remains at the apex of the liquid film until the bubble eventually ruptures, or the fiber begins to bend, thereby increasing curvature, and migrate down the cap toward the perimeter of the bubble where it remains bridged but bounded by a membrane of increasing thickness. If the fiber migrates to the perimeter of the liquid film, the fiber winds around the portion of the bubble that is extended above the undeformed surface of the bath, and forms a coil. A sequence of the winding process taken with an optical microscope from the above experiment is shown in Figs. 2(b)–2(g). For a fiber to spontaneously wrap around a bubble, the system must overcome the energy cost of bending around the perimeter of the liquid film atop the bubble, which is driven by a decrease in the system surface energy. We turn our attention first to the bending energy, before describing the surface energy.

When a fiber winds, it is observed to wind around the periphery of the bubble cap that extends above the surface of the liquid bath. We measure the radius of the bubble cap R_c by imaging the bubble from above with monochromatic light, resulting in a distinct light circle corresponding to the extended cap. An example of one of these images is shown in Figs. 3(a) and 3(b). Assuming linear elastic deformation of the fiber (typical strains <0.02 [29]), the bending energy *per unit length* for a fiber can be described with the Euler–Bernoulli beam theory,

$$E_b = \frac{\pi E r^4}{8R^2}, \tag{1}$$

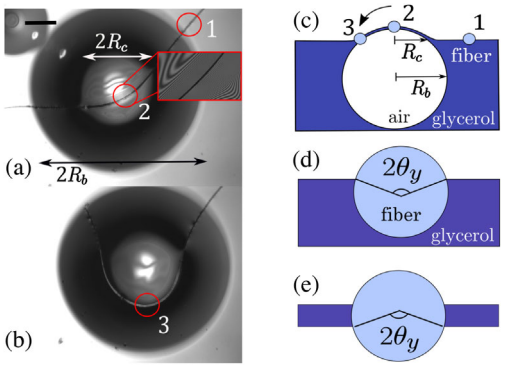

FIG. 3. (a),(b) Top-down, monochromatic optical images of a fiber-bubble system before and after migrating to the perimeter of the bubble cap. Red circles are numbered 1–3 and correspond to the different states of a segment of fiber shown in (c). The scale bar is 250 μm. Inset: interference fringes from the meniscus surrounding the bridged fiber. (c) Schematic of the fiber-bubble system side-on. The fiber is shown in light blue in position 1, 2, and 3, representing the unbridged, prewinding and postwinding positions of the fiber. (d),(e) Schematics of a fiber cross section floating on a fluid bath (unbridged), and bridged across a fluid membrane respectively. The schematic in (e) omits the bridging meniscus for clarity.

when the fiber bends to a radius of curvature R. As the fiber winds, it takes on a radius of curvature $R = R_c$, resulting in an increase in bending energy.

Bending in the fiber will only proceed spontaneously if the system free energy is reduced. Here the bending is accompanied by a reduction of interfacial energy associated with the fiber bridging the liquid film at the apex of the bubble. The liquid membrane at the apex of the air bubble is an air-glycerol-air film shown schematically in Fig. 3(c). The film is the region where the air bubble extends above the surface of the bath. The curvature of the membrane causes liquid to drain from the cap back into the bath, resulting in radial thinning of the cap. When the cap thins sufficiently, a fiber laid across the cap may "bridge" or straddle the liquid membrane, trading solid-liquid interface for liquid-vapor interface. This is observed experimentally as the fiber suddenly sinking into the liquid membrane, and the appearance of interference fringes resulting from a small meniscus that is created along the length of the fiber when viewed with monochromatic light. An example of these interference patterns are visible in the inset of Fig. 3(a), and an idealized schematic of a fiber before and after bridging is shown in Figs. 3(d) and 3(e). The bridging process occurs if there is a net reduction of interfacial energy *per unit length* of fiber which is given by

$$\Delta E_s = 2r\theta_y(\gamma_{sv} - \gamma_{sl}), \tag{2}$$

where θ_y is the glycerol-fiber contact angle, γ_{sv} is the solid-vapor interfacial tension, and γ_{sl} is the solid-liquid interfacial tension. The term on the right corresponds to the change in interfacial energy on the part of the fiber that bridges across the liquid membrane and goes from a solid-liquid interface to a solid-vapor interface. When $\gamma_{sv} - \gamma_{sl} < 0$, surface energy is reduced when the fiber bridges the liquid membrane. Using Young's law for partial wetting, $\gamma_{sv} = \gamma_{sl} + \gamma\cos\theta_y$, Eq. (2) can be rewritten as

$$\Delta E_s = 2r\gamma\theta_y\cos(\theta_y). \tag{3}$$

Since the thickness of the liquid membrane defining the air bubble increases radially from the center of the bubble, there will be a point where the liquid membrane is too thick for the fiber to bridge. At this point, the change in surface energy per unit length of fiber ΔE_s results in a driving force, pulling more fiber on to the air bubble and into the bridged state. As more fiber is pulled on to the air bubble, the fiber must bend and reorient to accommodate this extra length. Wrapping around the perimeter of the liquid membrane allows more fiber to bridge. Figures 3(a) and 3(b) show a top view of a fiber-bubble system before and after the fiber migrates to the perimeter of the air bubble, immediately before the fiber begins to wind around the perimeter of the membrane. Thus, we have the remarkable result that a fiber will wrap itself around the capped film at the apex of the bubble when the increase in bending energy is less than the decrease in interfacial energy (see video in the Supplemental Material [29]). Although the driving force causing this spontaneous winding comes from the bridging phenomenon, bridging alone is not sufficient to initiate winding, and many bridged samples do not proceed to wind. The energy released through bridging must be sufficient to overcome the increase in bending energy during the winding process.

We formulate a simple model by taking the initial state of the fiber as unbridged and straight [Fig. 3(d)], and comparing the energy to the final state of the fiber which bridges the liquid film and is bent around the perimeter of the bubble cap [Fig. 3(e)]. The critical radius of the bubble cap, $\mathcal{R}_c$, that distinguishes the nonwinding regime, $R < \mathcal{R}_c$, from the winding regime, $R > \mathcal{R}_c$, is given by the point where the change in bending energy is balanced by a change in surface energy: $\Delta E_s + \Delta E_b = 0$. We obtain $2r\gamma(\theta_y\cos\theta_y) = \pi E r^4/8\mathcal{R}_c^2$. Rearranging this expression allows one to calculate $\mathcal{R}_c$ as a function of l_b and θ_y,

$$\mathcal{R}_c = \frac{l_b}{\sqrt{2\theta_y\cos\theta_y}}. \tag{4}$$

Since θ_y is different for different polymer-liquid combinations, contact angle measurements were performed by placing small droplets of glycerol on films of each material. Droplets were imaged from the side to determine the contact angle θ_y for each polymer. The contact angles were $78° \pm 2°$, $82.5° \pm 3°$, and $67.5° \pm 3°$ for PS, SIS, and Elastollan, respectively [29].

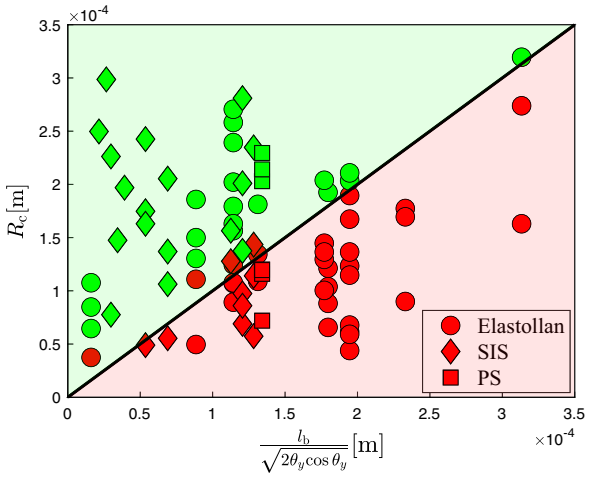

FIG. 4. Phase diagram of the winding criterion for Elastollan (circles), SIS (diamonds), and PS (triangles) fibers in glycerol. The slope defining the transition from Eq. (4) is $m = 1$. Green (light gray) points designate fiber-bubble combinations which wind, and red (dark gray) points designate those that do not wind.

Equation (4) was tested by observing fibers and bubbles of various sizes as they were brought into contact. After bridging, if the fiber migrated to the perimeter of the cap and continued to pull more fiber onto the cap, it was considered to have begun winding, and the point was plotted in green (light gray) in Fig. 4. Otherwise, if the fiber came to rest without winding around the perimeter, the point was plotted in red (dark gray). If any result was ambiguous (for example the bubble bursts while the fiber is migrating but has not begun to wind), the experiment was discarded. Notably, bubbles could be expected to burst prematurely if the time required to wind is longer than the typical lifespan of a bubble. Although the winding speed is expected to depend on the energy balance described above, the dynamics of the process is also related to the length of the fiber away from the bubble and the viscous drag this segment of fiber experiences. For this reason, the ability to see winding should be taken as an upper bound. By plotting R_c as a function of $l_b/\sqrt{2\theta_y \cos\theta_y}$ as suggested by Eq. (4), we obtain a winding phase diagram for all data with different bubble size, fiber radius, and three polymers spanning several orders of magnitude in modulus. The data are in excellent agreement with the model with a line passing through the origin and a slope of 1, defining the winding/no-winding boundary. The phase diagram indicates that winding is possible for bubbles with large radii and thin fibers, whereas thick fibers will not wind around a small radius.

Fibers that had completely wrapped around the bubble resulted in 2D coils as shown in Fig. 1(a) (video in the Supplemental Material [29]). By winding around the bubble cap, the fiber creates a spontaneous barrier which impedes drainage from the bubble cap to the bath. Thinning of the membrane is hindered, which enhances bubble stability. Though bubble stabilization depends on the viscosity of the liquid, winding speed, evaporation rate, and details as to how curved liquid membranes drain, we observe a qualitative increase of bubble lifetime. To test this, the lifetime of 20 bubbles with radii of 170–600 μm was measured without coils and found to be 110 ± 50 s. In contrast, for 22 similarly sized bubbles, fibers with radii of 2–11 μm were allowed to wind, and the wound bubbles were observed to have a lifetime of 440 ± 190 s, even *after* the winding was complete (a process that takes approximately 1–2 minutes). Since the winding process is dependent on the fiber thickness and bubble radius, the lifetime of wound bubbles presented should be taken as a lower bound. In fact, some bubbles survived hours, which is consistent with the stabilizing qualities of Pickering emulsions [48].

FIG. 5. A macroscopic demonstration of how the fiber coil can collapse to a flat surface, forming a unique, noncircular shape.

In instances when the fiber is thin and long, and the air bubble is large, the fiber migration process creates an S-shaped curve at the apex [see Fig. 1(a)]. The S-shaped curve is formed when the length of fiber extending from both sides of the bubble is long. In that case, an S-shaped curve must appear to satisfy the fiber lying on a 2D surface and winding in the same orientation (see the Supplemental Material [29]). Figure 1(b) shows the shape the fiber coil took after the bubble burst, and demonstrates another interesting aspect of the fiber coil geometry that is produced through winding. As a fiber completely surrounds a bubble cap, pulling more fiber onto the bubble perimeter requires the existing coil to be displaced. By migrating up the cap, more area around the perimeter of the cap can be liberated. The result is a coil which begins to trace the three-dimensional surface area of the spherical cap. When the bubble finally bursts, if there is low fiber-fiber adhesion, the coil will violently unwind in a process similar to the "entropic explosion" seen in viral capsids [39–42]. If there is sufficient adhesion between fiber surfaces, capillary forces pull the coil onto the surface of the bath, forcing the coil, which conforms to a spherical cap, to collapse onto an unfavorable flat surface. The deformation results in the unique shape shown in Fig. 1(b). One can replicate this easily by winding a rope around the apex of a sphere, and collapsing the structure onto a flat surface as shown in Fig. 5.

Here a unique self-assembly process is presented which occurs when thin polymer fibers are brought in contact with air bubbles located at the surface of a liquid bath. Fibers were found to bridge the liquid membrane defined by the

air-liquid-air interface of the air bubble at the surface of the bath. Doing so reduces the interfacial energy of the fiber-liquid system. The decrease in interfacial energy of the system comes at a cost of increasing the bending energy of the fiber as more fiber is pulled into the bridged state and forced to reorient on the bubble cap. A simple expression depending on the bubble size, bending elastocapillary length l_b, and liquid-solid contact angle of the fiber predicts the onset of this spontaneous winding process. This expression was confirmed experimentally for fibers of various sizes and materials in a bath of glycerol. By wrapping a bubble cap with a spiral of fiber, the flow of liquid from the cap back into the bath is impeded which significantly increases bubble lifetimes. The self-assembly process may be used in the fabrication of 2D microcoils, the production of metamaterials, or harnessed to stabilize or pattern microbubbles.

We gratefully acknowledge financial support by the Natural Science and Engineering Research Council of Canada.

*dalnoki@mcmaster.ca

[1] J. Bico, B. Roman, L. Moulin, and A. Boudaoud, Elasto-capillary coalescence in wet hair, Nature (London) **432**, 690 (2004).
[2] C. Duprat, S. Protiére, A. Y. Beebe, and H. A. Stone, Wetting of flexible fibre arrays, Nature (London) **482**, 510 (2012).
[3] C. Duprat and S. Protiere, Capillary stretching of fibers, Europhys. Lett. **111**, 56006 (2015).
[4] A. Sauret, F. Boulogne, D. Cébron, E. Dressaire, and H. A. Stone, Wetting morphologies on an array of fibers of different radii, Soft Matter **11**, 4034 (2015).
[5] H. Elettro, A. Antkowiak, and S. Neukirch, The heavy windlass: Buckling and coiling of an elastic rod inside a liquid drop in the presence of gravity, Mech. Res. Commun. **93**, 58 (2018).
[6] G McHale, N. A. Käb, M. I. Newton, and S. M. Rowan, Wetting of a high-energy fiber surface, J. Colloid Interface Sci. **186**, 453 (1997).
[7] B. J. Carroll, The equilibrium of liquid drops on smooth and rough circular cylinders, J. Colloid Interface Sci. **97**, 195 (1984).
[8] D. Quéré, Fluid coating on a fiber, Annu. Rev. Fluid Mech. **31**, 347 (1999).
[9] O. Campás, T. Mammoto, S. Hasso, R. A. Sperling, D. O'Connell, A. G. Bischof, R. Maas, D. A. Weitz, L. Mahadevan, and D. E. Ingber, Quantifying cell-generated mechanical forces within living embryonic tissues, Nat. Methods **11**, 183 (2014).
[10] J. B. Grotberg and O. E. Jensen, Biofluid mechanics in flexible tubes, Annu. Rev. Fluid Mech. **36**, 121 (2004).
[11] A. L. Hazel and M. Heil, Surface-tension-induced buckling of liquid-lined elastic tubes: a model for pulmonary airway closure, Proc. R. Soc. A **461**, 1847 (2005).
[12] B. Roman and J. Bico, Elasto-capillarity: Deforming an elastic structure with a liquid droplet, J. Phys. Condens. Matter **22**, 493101 (2010).
[13] S. Shojaei-Zadeh, S. R. Swanson, and S. L. Anna, Highly uniform micro-cavity arrays in flexible elastomer film, Soft Matter **5**, 743 (2009).
[14] R. W. Style, R. Boltyanskiy, Y. Che, J. S. Wettlaufer, L. A. Wilen, and E. R. Dufresne, Universal Deformation of Soft Substrates Near a Contact Line and the Direct Measurement of Solid Surface Stresses, Phys. Rev. Lett. **110** (2013).
[15] A. Chakrabarti and M. K. Chaudhury, Direct measurement of the surface tension of a soft elastic hydrogel: Exploration of elastocapillary instability in adhesion, Langmuir **29**, 6926 (2013).
[16] J. Bico, É. Reyssat, and B. Roman, Elastocapillarity: When surface tension deforms elastic solids, Annu. Rev. Fluid Mech. **50**, 629 (2018).
[17] A. E. Cohen and L. Mahadevan, Kinks, rings, and rackets in filamentous structures, Proc. Natl. Acad. Sci. U.S.A. **100**, 12141 (2003).
[18] B. J. Carroll, The accurate measurement of contact angle, phase contact areas, drop volume, and Laplace excess pressure in drop-on-fiber systems, J. Colloid Interface Sci. **57**, 488 (1976).
[19] G. McHale and M. I. Newton, Global geometry and the equilibrium shapes of liquid drops on fibers, Colloids Surf., A **206**, 79 (2002).
[20] T. H. Chou, S. J. Hong, Y. E. Liang, H. K. Tsao, and Y. J. Sheng, Equilibrium phase diagram of drop-on-fiber: Coexistent states and gravity effect, Langmuir **27**, 3685 (2011).
[21] A. Sauret, F. Boulogne, K. Somszor, E. Dressaire, and H. A. Stone, Drop morphologies on flexible fibers: Influence of elastocapillary effects, Soft Matter **13**, 134 (2017).
[22] H. Elettro, F. Vollrath, A. Antkowiak, and S. Neukirch, Drop-on-coilable-fibre systems exhibit negative stiffness events and transitions in coiling morphology, Soft Matter **13**, 5509 (2017).
[23] P. Grandgeorge, A. Antkowiak, and S. Neukirch, Auxiliary soft beam for the amplification of the elasto-capillary coiling: Towards stretchable electronics, Adv. Colloid Interface Sci. **255**, 2 (2018).
[24] Q. Liu and B. Xu, Liquid-evaporation-assisted self-folding of one-dimensional nanomaterials, J. Phys. Chem. C **122**, 3078 (2018).
[25] H. Elettro, S. Neukirch, F. Vollrath, and A. Antkowiak, In-drop capillary spolling of spider capture thread inspires hybrid fibers with mixed solid-liquid mechanical properties, Proc. Natl. Acad. Sci. U.S.A. **113**, 6143 (2016).
[26] H. Elettro, F. Vollrath, A. Antkowiak, and S. Neukirch, Coiling of an elastic beam inside a disk: A model for spider-capture silk, Int. J. Nonlinear Mech. **75**, 59 (2015).
[27] A. Fargette, S. Neukirch, and A. Antkowiak, Elastocapillary Snapping: Capillarity Induces Snap-Through Instabilities in Small Elastic Beams, Phys. Rev. Lett. **112** (2014).
[28] R. D. Schulman, A. Porat, K. Charlesworth, A. Fortais, T. Salez, E. Raphaël, and K. Dalnoki-Veress, Elastocapillary bending of microfibers around liquid droplets, Soft Matter **13**, 720 (2017).

[29] See Supplemental Materials at http://link.aps.org/supplemental/10.1103/PhysRevLett.127.218001 for spontaneous elastocapillary winding of thin elastic fibers in contact with bubbles.
[30] G. Morris, K. Hadler, and J. Cilliers, Particles in thin liquid films and at interfaces, Curr. Opin. Colloid Interface Sci. **20**, 98 (2015).
[31] S. A. Ali, P. A. Gauglitz, and W. R. Rossen, Stability of Solids-Coated Liquid Layers between Bubbles, Ind. Eng. Chem. Res. **39**, 2742 (2000).
[32] T Horozov, Foams and foam films stabilised by solid particles, Curr. Opin. Colloid Interface Sci. **13**, 134 (2008).
[33] G. Bournival, S. Ata, and E. J. Wanless, The roles of particles in multiphase processes: Particles on bubble surfaces, Adv. Colloid Interface Sci. **225**, 114 (2015).
[34] I. Capron and B. Cathala, Surfactant-free high internal phase emulsions stabilized by cellulose nanocrystals, Biomacromolecules **14**, 291 (2013).
[35] S. Lam, K. P. Velikov, and O. D. Velev, Pickering stabilization of foams and emulsions with particles of biological origin, Curr. Opin. Colloid Interface Sci. **19**, 490 (2014).
[36] A. M. Al-Qararah, T. Hjelt, A. Koponen, A. Harlin, and J. A. Ketoja, Bubble size and air content of wet fibre foams in axial mixing with macro-instabilities, Colloids Surf., A **436**, 1130 (2013).
[37] I. Kalashnikova, H. Bizot, P. Bertoncini, B. Cathala, and I. Capron, Cellulosic nanorods of various aspect ratios for oil in water Pickering emulsions, Soft Matter **9**, 952 (2013).
[38] T. Winuprasith and M. Suphantharika, Microfibrillated cellulose from mangosteen (Garcinia mangostana L.) rind: Preparation, characterization, and evaluation as an emulsion stabilizer, Food Hydrocolloids **32**, 383 (2013).
[39] A. S. Petrov and S. C. Harvey, Packaging double-helical DNA into viral capsids: Structures, forces, and energetics, Biophys. J. **95**, 497 (2008).
[40] P. K. Purohit, M. M. Inamdar, P. D. Grayson, T. M. Squires, J. Kondev, and R. Phillips, Forces during bacteriophage DNA packaging and ejection, Biophys. J. **88**, 851 (2005).
[41] P. K. Purohit, J. Kondev, and R. Phillips, Mechanics of DNA packaging in viruses, Proc. Natl. Acad. Sci. U.S.A. **100**, 3173 (2003).
[42] S. Tzlil, J. T. Kindt, W. M. Gelbart, and A. Ben-Shaul, Forces and pressures in DNA packaging and release from viral capsids, Biophys. J. **84**, 1616 (2003).
[43] Y. Toba, Drop production by bursting of air bubbles on the sea surface (II) theoretical study on the shape of floating bubbles, J. Oceanogr. Soc. Jpn. **15**, 121 (1959).
[44] C. T. Nguyen, H. M. Gonnermann, Y. Chen, C. Huber, A. A. Maiorano, A. Gouldstone, and J. Dufek, Film drainage and the lifetime of bubbles, Geochem. Geophys. Geosyst. **14**, 3616 (2013).
[45] P. L. L. Walls, L. Henaux, and J. C. Bird, Jet drops from bursting bubbles: How gravity and viscosity couple to inhibit droplet production, Phys. Rev. E **92**, 021002 (2015).
[46] R. D. Schulman and K. Dalnoki-Veress, Liquid Droplets on a Highly Deformable Membrane, Phys. Rev. Lett. **115**, 206101 (2015).
[47] J. Brandrup, E. H. Immergut, and E. A. Grulke, *Polymer Handbook*, 4th ed. (Wiley, New York, 1999).
[48] Y. Yang, Z. Fang, X. Chen, W. Zhang, Y. Xie, Y. Chen, Z. Liu, and W. Yuan, An overview of pickering emulsions: Solid-particle materials, classification, morphology, and applications, Front. Pharma. **8**, 287 (2017).